

Deep Learning the Hohenberg-Kohn Maps of Density Functional Theory

Javier Robledo Moreno ^{1,2,*}, Giuseppe Carleo ^{1,†} and Antoine Georges ^{1,3,4,5,‡}

¹Center for Computational Quantum Physics, Flatiron Institute, New York, New York 10010, USA

²Center for Quantum Phenomena, Department of Physics, New York University, 726 Broadway, New York, New York 10003, USA

³Collège de France, 11 place Marcelin Berthelot, 75005 Paris, France

⁴CPHT, CNRS, École Polytechnique, IP Paris, F-91128 Palaiseau, France

⁵DQMP, Université de Genève, 24 quai Ernest Ansermet, CH-1211 Genève, Suisse



(Received 7 November 2019; accepted 14 July 2020; published 12 August 2020)

A striking consequence of the Hohenberg-Kohn theorem of density functional theory is the existence of a bijection between the local density and the ground-state many-body wave function. Here we study the problem of constructing approximations to the Hohenberg-Kohn map using a statistical learning approach. Using supervised deep learning with synthetic data, we show that this map can be accurately constructed for a chain of one-dimensional interacting spinless fermions in different phases of this model including the charge ordered Mott insulator and metallic phases and the critical point separating them. However, we also find that the learning is less effective across quantum phase transitions, suggesting an intrinsic difficulty in efficiently learning nonsmooth functional relations. We further study the problem of directly reconstructing complex observables from simple local density measurements, proposing a scheme amenable to statistical learning from experimental data.

DOI: [10.1103/PhysRevLett.125.076402](https://doi.org/10.1103/PhysRevLett.125.076402)

Introduction.—The Hohenberg-Kohn (HK) theorem [1] is a founding principle of density functional theory (DFT). It establishes that there exists a bijective map between the local density and the one-body potential. This, remarkably, also implies a bijective relation between the local density and the ground-state many-body wave function of the system $\psi(\mathbf{r}_1, \mathbf{r}_2, \dots, \mathbf{r}_N)$, which is thus a unique functional of the one-particle density $\rho(\mathbf{r})$. Hence, there is also an injective map connecting the local density with any observable of interest (such as two-point density correlation functions) in the ground state:

$$\rho(\mathbf{r}) \xleftrightarrow{\text{DTWF}} \psi(\mathbf{r}_1, \mathbf{r}_2, \dots) \longrightarrow \langle n(\mathbf{r})n(\mathbf{r}') \rangle_\psi$$



where DTWF is the density to ground-state wave function map and DTCF labels the density to two-point density correlator map. However, the exact form of the DTWF and DTCF maps is unknown in most cases [2,3] and phenomenological approximations are required to construct them. These approximations typically lead to inaccurate predictions when the electrons are strongly correlated [4,5], as in Mott insulating phases.

With the recent interest in machine learning (ML) techniques applied to physical sciences [6], data-driven approaches have successfully been applied to DFT for different applications. Some works use ML techniques in the Kohn-Sham (KS) scheme [7], to improve or

parametrize exchange-correlation functionals and potentials [8–14], the noninteracting kinetic energy functionals and their derivatives [8,15–18] or the full density functional [18–20]. Other works take a more direct approach based on the HK theorem to learn the potential to density map and the potential to ground-state energy map [21], potential to energy spectrum map [22], infer relevant energies of the system from the local density [23] or the external potential [24]. Despite this progress, little is known about the practical computational complexity of the statistical learning of the direct DTWF and DTCF HK maps, and in what regimes the learning approach can fail.

In this Letter, we systematically investigate the problem of reconstructing the ground-state wave function (DTWF) and the correlation functions (DTCF) from the knowledge of the local density, using supervised deep learning. Focusing on a lattice model of interacting electrons, we show that the DTWF map can be learned for different phases of the model, including Mott and metallic phases and the critical point. The explicit ML representation of the DTWF map allows for the possibility to gain insight into this high dimensional bijection and its properties in models with finite basis sets such as small molecules. In particular, we find that learning the map through a quantum phase transition (QPT) leads to intrinsic representational difficulties. Finally, we show that the DTCF map allows one to compute physical quantities of interest—like two-point correlators—and their scaling laws directly from the local density of the system. Specifically, we could extract the Luttinger liquid (LL) parameter, finite-size scaling

behavior, and logarithmic corrections from the ML-constructed correlation functions. This opens the possibility of reconstructing nontrivial physical quantities directly from experimental x-ray measurements of the electron density [25,26], or learning these maps from quantum simulation experiments [27–34].

The Hohenberg-Kohn theorem.—The fundamental theorem of DFT is formulated in the context of interacting electrons subjected to an external potential $v(\mathbf{r})$, whose Hamiltonian has the form

$$\hat{H} = \hat{K} + \hat{U} + \hat{V}, \quad (1)$$

where \hat{K} is the kinetic energy operator, \hat{U} are the two-body interactions, and \hat{V} is the one-body external potential. For fixed \hat{K} and \hat{U} , the HK theorem states that there is a one-to-one correspondence between the local electron density in the ground-state $\rho(\mathbf{r})$ and the external potential $v(\mathbf{r})$.

Given the generality of this theorem, we consider in this work a Hamiltonian which is simpler than the full inhomogeneous electron gas, but has a structure similar to Eq. (1), namely, a 1D extended Hubbard model of spinless Fermions in a lattice of N sites with periodic boundary conditions:

$$H = \underbrace{-t \sum_i [c^\dagger(x_i)c(x_{i+1}) + \text{H.c.}]}_{\hat{K}} + \underbrace{U \sum_i n(x_i)n(x_{i+1})}_{\hat{U}} - \underbrace{\sum_i [v(x_i) + \mu]n(x_i)}_{\hat{V}}, \quad (2)$$

where $c^\dagger(x_i)$ and $c(x_i)$ are the Fermion creation and annihilation operators acting on lattice sites x_i and $n(x_i) = c^\dagger(x_i)c(x_i)$. t is the hopping amplitude, U is the density-density interaction, $v(x_i)$ is the external potential, and μ is the chemical potential. Throughout this work, we will consider the case when $t = 1$ and $U = \mu$, corresponding to an occupancy of one particle per two sites on average (half-filled band). A straightforward extension of the HK theorem to this model establishes that, on finite systems, the ground-state wave function components are a unique function of the local density $\rho_i = \langle \psi | n(x_i) | \psi \rangle$.

In the absence of an external potential, the model in Eq. (2) has a phase transition at $U/t = 2$ of the Kosterlitz-Thoules type [35]. For $U/t > 2$ the system is in the Mott insulator gapped phase, which is a long-range ordered charge density wave phase with spatial period $2a$, where a

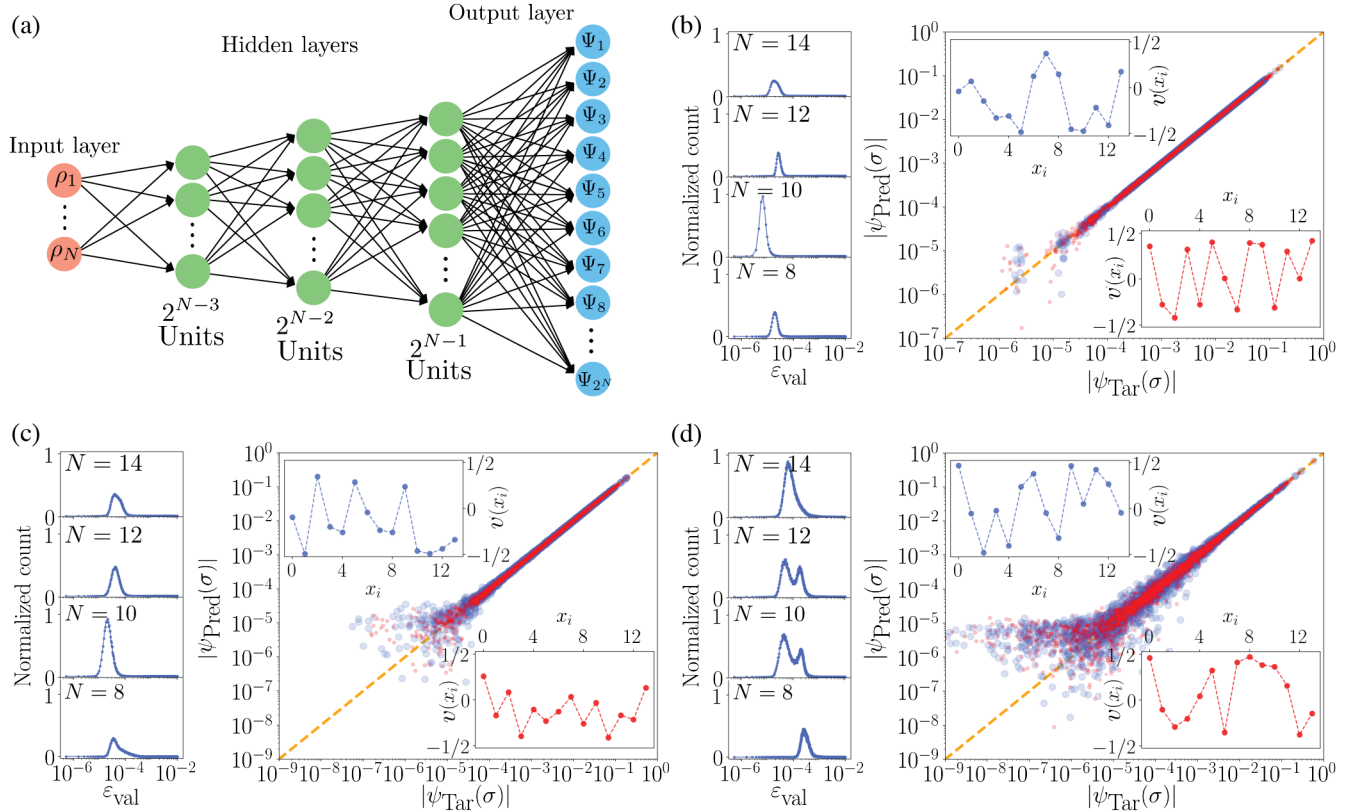


FIG. 1. (a) Diagram of the neural network architecture used to represent the $\rho_i \rightarrow |\psi\rangle$ (DTWF) map. (b) $U/t = 1$ (metal), (c) $U/t = 2$ (critical), (d) $U/t = 4$ (Mott insulator). Left: Normalized histograms of the error functions as defined in Eq. (4) over the validation set. Right: Predicted versus exact wave function components in the occupation number basis, given two different random potentials depicted in the insets. System size is $N = 14$. Red dots correspond to the potential in the inset in the lower right corner and blue ones to the potential in the upper left inset.

is the lattice constant. For $U/t < 2$ the system is a gapless LL metal [36,37] characterized by power-law decaying correlation functions:

$$\langle n(x_i)n(x_{i+l}) \rangle \sim \frac{C_1}{l^2} + \frac{C_2(-1)^l}{l^{2K}}, \quad (3)$$

where C_i are nonuniversal amplitudes and K is the LL parameter, which is known exactly from Bethe ansatz: $1/K = (2/\pi) \arccos(-U/2t)$ [38]. The critical point follows the same scaling with an additional $\sqrt{\log(c\ell)}$ contribution multiplying the staggered term [38,39].

Density to wave function map.—First, we study the possibility of learning the DTWF map using a deep fully connected feed-forward neural network [40]. We consider finite-size systems with $N = 7$ to $N = 14$ lattice sites. The input to the network is the N values of the local density ρ_i and the output are the 2^N components of the ground-state wave function $\psi(\sigma)$ in the occupation basis: $|\psi\rangle = \sum_{\sigma} \psi(\sigma)|\sigma\rangle$, where $\sigma \equiv \{n_1, \dots, n_N : n_i = 0, 1\}$ labels a specific occupation configuration. A representation of this architecture is shown in Fig. 1(a). All the layers are connected by the composition of an affine transformation and a nonlinear rectifier function, $\text{Relu}(x) = \max(0, x)$, except for the output layer, where the chosen nonlinearity enforces the normalization of the wave function—see Supplemental Material [41] for further information.

Supervised learning is used to find the set parameters of the network $\{\theta\}$ that minimize the infidelity of the wave function:

$$\varepsilon_{\text{train}}(\{\theta\}) = 1 - |\langle \psi_{\text{tar}} | \psi_{\text{pred}}(\{\theta\}) \rangle|, \quad (4)$$

where $|\psi_{\text{tar}}\rangle$ and $|\psi_{\text{pred}}\rangle$ are the target and predicted wave functions, respectively. For different U/t values, different networks are trained using a set of ground-state wave functions corresponding to Hamiltonians of the form of Eq. (2), with uniformly sampled random potentials with the restriction $|v(x_i)| \leq 1/2$. This ensures that the training set is not biased. The size of the training set is chosen to

increase linearly with system size. The construction of the density function is tested in the two phases of the system $U/t = 1$ (metallic), $U/t = 4$ (Mott insulator), and at the critical point $U/t = 2$. The accuracy of the learning is tested on a validation set, as per standard machine-learning practice [40]. We also test the capability of the ML-constructed wave functions to reconstruct the corresponding local densities and ground-state energies—see Supplemental Material [41].

The left panels in Figs 1(b)–1(d) show histograms of the error, as defined in Eq. (4), when constructing the wave function over the validation set for different values of U/t . The right panel shows correlation plots of exact versus ML-constructed wave function weights given two random potentials depicted in the insets. The histograms show narrow peaked error distributions. The position of the peak is not strongly affected by the system size or the value of U/t . In all of the cases the peak is centered around error values no larger than $\varepsilon_{\text{validation}} = 3.10^{-4}$ (overlaps of $|\langle \psi_{\text{tar}} | \psi_{\text{pred}} \rangle| = 0.9997$). The correlation plots show that the network can accurately predict all of the wave function components, without displaying significant deviations—outside rounding errors. Achieving a high degree of accuracy on examples not present in the training set is an indication that the network has not been overfitted, and indeed captures the underlying connection between the local density and the ground-state wave function.

We also test the neural network on a collection of “structured” (i.e., nonrandom) potentials, which are highly unlikely to belong to the training set. The potentials tested are sketched in Fig. 2(a) in a lattice with $N = 14$ sites. Figure 2(b) displays the error—as defined in Eq. (4)—as a function of N for the different potentials tested at the critical point $U/t = 2$. Except for the staggered potential, where the error is up to 2 orders of magnitude larger than the typical errors in the validation sets, all of the other cases display errors that are of the same order of magnitude as the ones found in the validation sets.

Learnability across a quantum phase transition.—The lack of accuracy found in the staggered potential case is

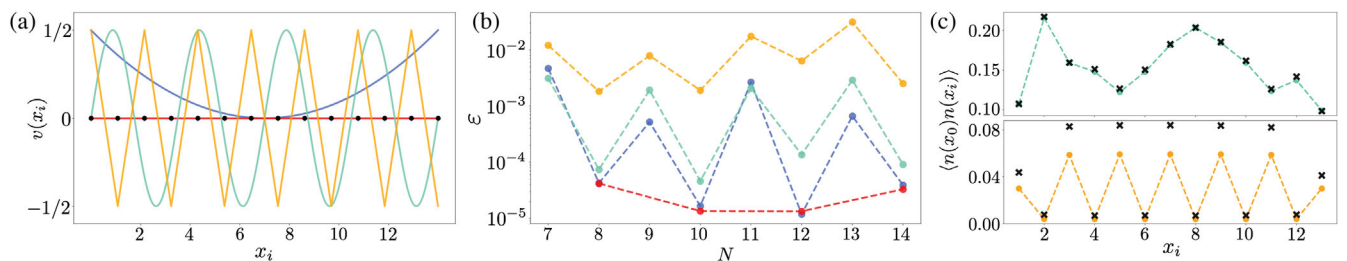


FIG. 2. Performance of the network in structured potentials. (a) Sketch of the tested potentials in a lattice with $N = 14$ sites. Potentials are quadratic (blue), no potential^{ma} (red), periodic with period $N/4$ (green), and staggered (orange). Black dots represent the position of the lattice sites. Panels (b) and (c) follow the same color code. (b) Error as defined in Eq. (4), as a function of the system size, when predicting the ground-state wave function given the potentials in panel (a). (c) Two-point density correlation functions computed from exact (dots connect by dashed lines) and ML-predicted (black crosses) wave functions. Only results for an even number of lattice sites are shown in this case as the ground state with an odd number of sites is degenerate.

striking and points to a likely fundamental difficulty in the description of this specific regime. The quantitative and qualitative loss of accuracy in the learned DTWF map is particularly evident in two-point correlation functions, as displayed in Fig. 2(c). This means that in the staggered case, the proposed ML architecture and training method are not capable of capturing the behavior of the DTWF map in this region of the space of applied potentials. Similar results are found in the metallic and Mott phases—see Supplemental Material [41].

To make sense of these discrepancies, we notice that the staggered potential stands on different physical grounds than the other structured cases analyzed. In this one-dimensional system, an infinitesimally small staggered potential induces a QPT corresponding to the opening of a gap, in turn leading to staggered ordering of the local density [38]. More generally, this QPT is driven by the amplitude λ of the staggered potential. In the small λ limit, $\rho_i = \rho_s(-1)^i$ with $\rho_s \propto \lambda^\mu$ the staggered density. For the U/t values analyzed in this work $\mu < 1$ [38]. Therefore, the derivative of the density with respect to the amplitude of the staggered potential diverges at the critical point. In the context of DFT, this means that the functional is not smooth in the presence of a QPT, since the density functional is constructed by a Legendre transformation from the potential, and the dependence of the density on the potential is nonanalytic in this case. This nonanalytic behavior leads to an intrinsic difficulty in learning the map using smooth functional approximations—such as neural networks—and unbiased sampling from random one-body potentials.

Density to correlation functions map.—Even in those regimes where the DTWF map is efficiently learned, the practical implementation of the statistical learning scheme is constrained to small systems by the exponential growth of the wave function with the number of lattice sites. As an alternative, here we explore the possibility of directly constructing the DTCF map with deep convolutional

networks, whose size does not scale exponentially with system size. They allow us to bypass the construction of the exponentially large wave function to directly compute observables of interest, in this case density-density correlators. The input of the convolutional network is the N values of ρ_i . The output is the $(N^2 - N)/2$ different pairs of correlation functions of the system. The chosen architecture consists of six convolutional layers with N filters each. The size of the kernel of the convolutions is 2. All of the convolutional layers use a Relu activation function. After the last convolutional layer, the output of the filters was flattened and connected using a fully connected layer with a Sigmoid(x) = $1/(1 + e^{-x})$ activation function. The architecture is shown in panel (a) of Fig. 3. Significantly larger systems are studied in this case ranging from $N = 18$ to $N = 50$ lattice sites. The training sets were the same as the ones used in the previous section, but generated using density matrix renormalization group (DMRG) on ITensor [43]. The weights of the network are obtained by minimizing the relative error averaged over all the correlation pairs in each sample of the training set. Different networks are trained for the three different values of U/t . The performance of the networks is tested in the validation set—see Supplemental Material [41].

Figure 3(b) shows the value of exact versus ML-constructed two-point density correlation functions in a system with $N = 50$ lattice sites, given the random potential depicted in the inset, at three different values of U/t . The plot demonstrates that the convolutional network is capable of accurately finding the values of the correlation functions. Figure 3(c) shows the value of the LL exponent—see Eq. (3)—obtained from the DMRG and the ML-constructed density-density correlation functions for different values of U/t . The value of K is obtained from the power law behavior of the correlation functions after removing the C_1/l^2 background. The values of K obtained from the ML correlation functions are in good agreement

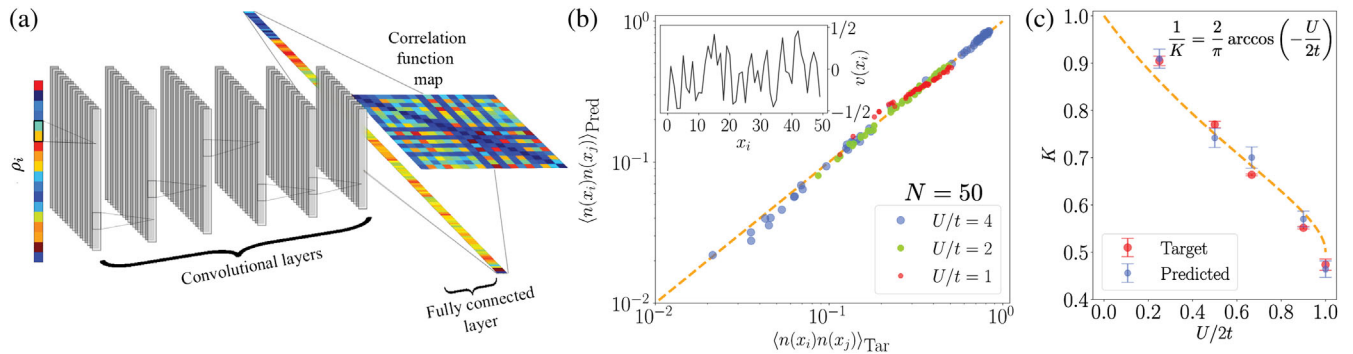


FIG. 3. (a) Scheme of the convolutional network used to represent the $\rho_i \rightarrow \langle n(x_i)n(x_k) \rangle$ (DTCF) map. The output of the network is sorted to produce the correlation function map. (b) Exact versus ML-constructed values of the two-point density correlation functions given the random potential shown in the inset, for different values of U/t in a lattice with $N = 50$ sites. Training sets are generated using DMRG in this case. (c) Luttinger liquid parameter as a function of $U/2t$. The dashed line shows the exact value from Bethe ansatz. Red dots correspond to the estimated value using DMRG in a lattice with $N = 50$ sites and blue dots correspond to the estimated value from the ML-predicted correlation functions.

with both the exact solution and the DMRG values (see Supplemental Material [41] for the raw data of the correlation functions). The small discrepancies arise from finite-size effects. Finite-size scaling allows us to capture more accurate estimates of K and the logarithmic correction in the critical point; see Ref. [41]. These results show that the construction of the exponentially large wave function can be bypassed to accurately reconstruct complex observables of interest and their scalings in the three regimes of (i) power-law decaying correlations, (ii) true long-range order, (iii) critical point between the two. The performance of this method is similar for $N = 18$ and $N = 50$ —see Supplemental Material [41]—demonstrating its scalability.

Conclusion.—In this Letter we proposed a method based on supervised training deep learning to successfully construct the local density to ground-state many-body wave function map and the local density to correlation functions maps for a model of interacting spinless Fermions in a 1D lattice. Hence, we provide evidence that machine learning tools provide a suitable framework to represent these high-dimensional density functionals in the two phases of the system, including the charge ordered Mott insulator and the critical point. The results serve as a proof of concept to open new lines of research where parameters from a suitable variational ansatz, such as neural network quantum states [44], could be predicted instead of the exponentially many wave function components. Thanks to the insight provided by the explicit construction of the DTWF map, we also found that the learning performance deteriorates through a quantum phase transition, due to the nonanalytic behavior of the density functional. Finally, it was shown that the (exponentially costly) reconstruction of the wave function can be bypassed to directly infer complex physical observables from the local density only. An interesting open research direction concerns the application of this idea to larger system sizes. Combining our approach with an intrinsic notion of locality in the correlations and the potential transfer of learning techniques could open the possibility to infer correlation functions in larger systems from learned features in smaller ones.

J. R. M. acknowledges support from the CCQ graduate fellowship in computational quantum physics. The Flatiron Institute is a division of the Simons Foundation. The authors acknowledge discussions with Stefano Baroni, Timothy Berkelbach, Kieron Burke, Thierry Giamarchi, Masatoshi Imada, James Stokes, and Miles Stoudenmire.

*jrm874@nyu.edu

†gcarleo@flatironinstitute.org

‡ageorges@flatironinstitute.org

- [1] P. Hohenberg and W. Kohn, *Phys. Rev.* **136**, B864 (1964).
 [2] A. J. Cohen, P. Mori-Sánchez, and W. Yang, *Chem. Rev.* **112**, 289 (2012).
 [3] W. Kohn, *Rev. Mod. Phys.* **71**, 1253 (1999).

- [4] A. J. Cohen, P. Mori-Sánchez, and W. Yang, *Science* **321**, 792 (2008).
 [5] P. Mori-Sánchez, A. J. Cohen, and W. Yang, *Phys. Rev. Lett.* **100**, 146401 (2008).
 [6] G. Carleo, I. Cirac, K. Cranmer, L. Daudet, M. Schuld, N. Tishby, L. Vogt-Maranto, and L. Zdeborová, *Rev. Mod. Phys.* **91**, 045002 (2019).
 [7] W. Kohn and L. J. Sham, *Phys. Rev.* **140**, A1133 (1965).
 [8] B. Kolb, L. C. Lentz, and A. M. Kolpak, *Sci. Rep.* **7**, 1192 (2017).
 [9] Q. Liu, J. Wang, P. Du, L. Hu, X. Zheng, and G. Chen, *J. Phys. Chem. A* **121**, 7273 (2017).
 [10] K. T. Lundgaard, J. Wellendorff, J. Voss, K. W. Jacobsen, and T. Bligaard, *Phys. Rev. B* **93**, 235162 (2016).
 [11] S. Pilati and P. Pieri, *Sci. Rep.* **9**, 5613 (2019).
 [12] J. Schmidt, C. L. Benavides-Riveros, and M. A. L. Marques, *J. Phys. Chem. Lett.* **10**, 6425 (2019).
 [13] R. Nagai, R. Akashi, S. Sasaki, and S. Tsuneyuki, *J. Chem. Phys.* **148**, 241737 (2018).
 [14] S. Dick and M. Fernandez-Serra, *Nat. Commun.* **11**, 3509 (2020).
 [15] P. Golub and S. Manzhos, *Phys. Chem. Chem. Phys.* **21**, 378 (2019).
 [16] J. Seino, R. Kageyama, M. Fujinami, Y. Ikabata, and H. Nakai, *J. Chem. Phys.* **148**, 241705 (2018).
 [17] J. C. Snyder, M. Rupp, K. Hansen, L. Blooston, K.-R. Müller, and K. Burke, *J. Chem. Phys.* **139**, 224104 (2013).
 [18] L. Li, J. C. Snyder, I. M. Pelaschier, J. Huang, U.-N. Niranjan, P. Duncan, M. Rupp, K.-R. Müller, and K. Burke, *Int. J. Quantum Chem.* **116**, 819 (2016).
 [19] J. C. Snyder, M. Rupp, K. Hansen, K.-R. Müller, and K. Burke, *Phys. Rev. Lett.* **108**, 253002 (2012).
 [20] L. Li, T. E. Baker, S. R. White, and K. Burke, *Phys. Rev. B* **94**, 245129 (2016).
 [21] F. Brockherde, L. Vogt, L. Li, M. E. Tuckerman, K. Burke, and K.-R. Müller, *Nat. Commun.* **8**, 872 (2017).
 [22] Q. Liu, J. Wang, P. Du, L. Hu, X. Zheng, and G. Chen, *J. Phys. Chem. A* **121**, 7273 (2017).
 [23] J. Nelson, R. Tiwari, and S. Sanvito, *Phys. Rev. B* **99**, 075132 (2019).
 [24] K. Ryczko, D. A. Strubbe, and I. Tamblyn, *Phys. Rev. A* **100**, 022512 (2019).
 [25] S. Grabowsky, A. Genoni, and H.-B. Bürgi, *Chem. Sci.* **8**, 4159 (2017).
 [26] K. Tolborg and B. B. Iversen, *Chem. Eur. J.* **25**, 15010 (2019).
 [27] J. E. Lye, L. Fallani, M. Modugno, D. S. Wiersma, C. Fort, and M. Inguscio, *Phys. Rev. Lett.* **95**, 070401 (2005).
 [28] M. White, M. Pasienski, D. McKay, S. Q. Zhou, D. Ceperley, and B. DeMarco, *Phys. Rev. Lett.* **102**, 055301 (2009).
 [29] A. Celi, B. Vermersch, O. Viyuela, H. Pichler, M. D. Lukin, and P. Zoller, *Phys. Rev. X* **10**, 021057 (2020).
 [30] A. Omran, H. Levine, A. Keesling, G. Semeghini, T. T. Wang, S. Ebadi, H. Bernien, A. S. Zibrov, H. Pichler, S. Choi *et al.*, *Science* **365**, 570 (2019).
 [31] A. Keesling, A. Omran, H. Levine, H. Bernien, H. Pichler, S. Choi, R. Samajdar, S. Schwartz, P. Silvi, S. Sachdev, P. Zoller, M. Endres, M. Greiner, V. Vuletic, and M. D. Lukin, *Nature (London)* **568**, 207 (2019).

- [32] I. Bloch, J. Dalibard, and W. Zwerger, *Rev. Mod. Phys.* **80**, 885 (2008).
- [33] S. Scherg, T. Kohlert, J. Herbrych, J. Stolpp, P. Bordia, U. Schneider, F. Heidrich-Meisner, I. Bloch, and M. Aidelsburger, *Phys. Rev. Lett.* **121**, 130402 (2018).
- [34] J. F. Sherson, C. Weitenberg, M. Endres, M. Cheneau, I. Bloch, and S. Kuhr, *Nature (London)* **467**, 68 (2010).
- [35] H. Mikeska and A. Kolezhuk, in *Quantum Magnetism*, edited by U. Schollwöck, J. Richter, D. J. J. Farnell, and R. F. Bishop, Lecture Notes in Physics Vol. 645 (Springer, Berlin, Heidelberg, 2004), pp. 1–38, <https://doi.org/10.1007/BFb0119591>.
- [36] J. M. Luttinger, *J. Math. Phys. (N.Y.)* **4**, 1154 (1963).
- [37] D. C. Mattis and E. H. Lieb, *J. Math. Phys. (N.Y.)* **6**, 304 (1965).
- [38] T. Giamarchi, *Quantum Physics in One Dimension*. (Oxford University Press, Oxford, 2003), pp. 160–199, <https://dx.doi.org/10.1093/acprof:oso/9780198525004.001.0001>.
- [39] K. A. Hallberg, P. Horsch, and G. Martínez, *Phys. Rev. B* **52**, R719 (1995).
- [40] I. Goodfellow, Y. Bengio, and A. Courville, *Deep Learning* (MIT Press, Massachusetts, 2016).
- [41] See Supplemental Material at <http://link.aps.org/supplemental/10.1103/PhysRevLett.125.076402> for information about the reconstruction of ground-state energies and densities from ML wave functions, performance of the DTWF for all U/t values tested across the considered phase transition, DTWF performance on the validation set and a detailed description of the finite-size scaling properties of the two-point density correlation functions and logarithmic corrections in the critical point, which includes Ref. [42].
- [42] T. A. Kaplan, P. Horsch, and J. Borysowicz, *Phys. Rev. B* **35**, 1877 (1987).
- [43] ITensor Library (version 2.0.11), <http://itensor.org>.
- [44] G. Carleo and M. Troyer, *Science* **355**, 602 (2017).